Propagation and Interaction of Cellular Fronts in a Closed System

M. Fuentes,[†] M. N. Kuperman,*[,†,‡] and P. De Kepper[‡]

Comisión Nacional de Energía Atómica, Centro Atómico Bariloche and Instituto Balseiro (CNEA and UNC), 8400 San Carlos de Bariloche, Argentina, and Centre de Recherche Paul Pascal, CNRS, Université Bordeaux I, Av. Schweitzer, 33600 Pessac, France

Received: October 10, 2000; In Final Form: April 25, 2001

We experimentally study the development of cellular acidity fronts during the chlorite oxidation of tetrationate performed in a thin layer of viscous solution containing different amounts of polyelectrolyte. These properties and the interaction between fronts are investigated as a function of initial chemical concentrations. The observations are compared to numerical results obtained with a skeleton kinetic model of the reaction using a two-dimensional finite element integration scheme. The agreements with observations are striking.

1. Introduction

The development of symmetry-breaking patterns in reaction−diffusion (R−D) systems with positive feedback is well-known. Their growth behavior and pattern selection mechanism are currently extensively studied both theoretically[1−4] and experimentally.[1,5−7] Among these, the lateral instability of planar fronts constitutes an interesting and yet rare example of a pattern formation mechanism, in isothermal wet chemistry. When an autocatalytic reaction takes place in an unstirred thin layer of solution propagating R−D fronts, separating regions with high concentrations of reactants and autocatalytic product, respectively, are generally observed. In batch, under normal conditions, an initially planar front propagates into the homogeneous reactant zone, maintaining its planar symmetry. However, it is theoretically expected that if the reactant diffuses faster than the autocatalytic species the front can lose its symmetry. In this case, a planar front loses its stability, yielding the formation of what is known as "cellular structures". The break of the planar symmetry is a consequence of the lateral instability of the front.[8,9] It is also theoretically shown that in effectively isothermal two-variable systems such instability can only develop when the system presents cubic autocatalytic kinetics.[10] In isothermal convection free solution chemistry, cellular fronts have been clearly observed in the iodate−arsenite,[11] chlorine dioxide−iodine−malonic acid,[12] and chlorite−tetrathionate systems.[13,14]

In this paper, we focus on hydrogen ion-catalyzed oxidation of tetrathionate by chlorite. The stoichiometry and an overall rare law were experimentally determined for the reaction, in the presence of excess chlorite:[15,16]

$$7ClO_2^- + 2S_4O_6^{2-} + 6H_2O \xrightarrow{[H^+]} 7Cl^- + 8SO_4^{2-} + 12H^+ \quad \text{(I)}$$

$$r = -\frac{1}{7}\frac{d[ClO_2^-]}{dt} = k[ClO_2^-][S_4O_6^{2-}][H^+]^2$$

They satisfy indeed the kinetic conditions: the rate law of the reaction shows second-order kinetics with the respect to the hydrogen ion, which plays the role of the autocatalyst.

However, another condition necessary for achieving the lateral destabilization of a planar front is that the reactants should diffuse faster than the autocatalyst. In aqueous solution, the mobility of hydrogen ions is about an order of magnitude greater than those of other small hydrated ions, but because the local electroneutrality of the solution must be preserved, the effective diffusion of the hydrogen ions does not differ much from that of the other counterions in the solution, contrary to what it often claimed. Still, to obtain lateral instability, the hydrogen ions must diffuse significantly slower than the reactants, the chlorite and the tetrathionate ions. This is made possible by introducing an immobile complexing agent that reversibly captures the hydrogen ions without directly interfering with the reaction.[17] This transient capture of the ions results in a slowing of its random walk, macroscopically affecting its diffusion coefficient. Experimentally, this was achieved by introducing in the solution large polymer chains containing carboxylic groups. In fact, the solutions were made viscous by incorporating polyacrylamide and controlled amounts of the acrylamide−methacrylate copolymer. This viscous solution ensures the elimination of undesirable convective effects and still acts as an aqueous medium for the small hydrated ions other than hydrogen ions. The carboxylic groups on the copolymer chains remain immobile and act as transitory fixed traps for the hydrogen ion, through standard reversible acid−base equilibrium. This process can be represented as

$$H^+ + -COO^- \rightleftharpoons -COOH \quad \text{(II)}$$

The procedure we followed is very similar to that described by Toth et al.[13] with some differences in the viscous medium put to use. Besides reproducing the results obtained in that work, we study the behavior of the cellular acidity front in relation with the concentration of the hydrogen ion complexing agent and that of the reactants. As in ref 18, we measure the front mean velocity and the mean size of the cellular structures. The novelty of the work presented here, besides the change introduced by the utilization of the viscous solution, resides in the fact that we study the propagation of fronts with circular geometry and also show evidence of their interaction. Finally, we compare the experimental results with that of numerical simulations.

[†] Centro Atómico Bariloche and Instituto Balseiro (CNEA and UNC).
[‡] Université Bordeaux I.

10.1021/jp0037192 CCC: $20.00
Published on Web 06/14/2001

2. The Model

As in refs 14 and 18, we consider a reaction−diffusion model described by nonlinear partial differential equations as follows:

$$\frac{\partial[ClO_2^-]}{\partial t} = D_1\nabla^2[ClO_2^-] - 7k[ClO_2^-][S_4O_6^{2-}][H^+]^2$$

$$\frac{\partial[S_4O_6^{2-}]}{\partial t} = D_1\nabla^2[S_4O_6^{2-}] - 2k[ClO_2^-][S_4O_6^{2-}][H^+]^2 \quad (1)$$

$$\frac{\partial[H^+]}{\partial t} = D_2\nabla^2[H^+] + 12k[ClO_2^-][S_4O_6^{2-}][H^+]^2$$

If we include the rapid equilibrium of hydrogen ions with fixed carboxylic groups as in eq II, this modifies the dynamical equation for free protons and introduces the protonated carboxylic groups as an additional variable. We then have

$$\frac{\partial[H^+]}{\partial t} = D_2\nabla^2[H^+] + 12k[ClO_2^-][S_4O_6^{2-}][H^+]^2 + k_-[-COOH] - k_+[-COO^-][H^+]$$

$$\frac{\partial[-COOH]}{\partial t} = D_3\nabla^2[-COOH] - k_-[-COOH] + k_+[-COO^-][H^+] \quad (2)$$

where $D_3 = 0$ because the carboxylic groups are bounded to the quasi-immobile polymer chains. Moreover, due to fast acid−base equilibrium, we have

$$k_+[-COO^-][H^+] = k_-[-COOH]$$

If $[-COO^-] \gg [-COOH]$, the system can be reduced by eliminating $[-COO^-]$ as an independent variable. We can derive the following proportionality relation

$$K[H^+] = [-COOH]$$

with

$$\frac{k_+}{k_-}[-COO^-] = K \quad (3)$$

If $[H]_T = [H^+] + [-COOH] = (1 + K)[H^+]$, the total available hydrogen ion concentration in the system, we have

$$\frac{\partial[H]_T}{\partial t} = (1+K)\frac{\partial[H^+]}{\partial t} = D_2\nabla^2[H^+] + 12k[ClO_2^-][S_4O_6^{2-}][H^+]^2 \quad (4)$$

and the new effective rate for free hydrogen ions becomes

$$\frac{\partial[H^+]}{\partial t} = \frac{D_2}{(1+K)}\nabla^2[H^+] + \frac{12k}{(1+K)}[ClO_2^-][S_4O_6^{2-}][H^+]^2 \quad (5)$$

We assume that the diffusion coefficients are the same for the reagents and that the relation

$$\frac{[ClO_2^-] - \xi[ClO_2^-]_i}{[S_4O_6^{2-}]} = {}^7/_2$$

holds throughout the whole experiment, where ξ is the stoichiometric excess of chlorite

$$\xi = 1 - \frac{7[S_4O_6^{2-}]_i}{2[ClO_2^-]_i}$$

and the subscript i denotes the initial concentration. Thus, we can write the concentration of tetrathionate in terms of that of chlorite

$$[S_4O_6^{2-}] = \frac{2}{7}([ClO_2^-] - \xi[ClO_2^-]_i) \quad (6)$$

eliminating the second equation in eq 1. Replacing the concentration of tetrathionate in eq 1 according to eq 6, we have

$$\frac{\partial\alpha}{\partial t} = D_1\nabla^2\alpha - 2\hat{k}(\alpha - \hat{\xi})\alpha\beta^2$$

$$\frac{\partial\beta}{\partial t} = \frac{1}{1+K}\left[D_2\nabla^2\beta + \frac{24}{7}\hat{k}(\alpha - \hat{\xi})\alpha\beta^2\right] \quad (7)$$

where $\alpha = [ClO_2^-]/[ClO_2^-]_0$, $\beta = [H^+]/[ClO_2^-]_0$, $\hat{k} = k/([ClO_2^-]_0)^3$, and $\hat{\xi} = \xi[ClO_2^-]_i/[ClO_2^-]_0$. We normalize the concentrations α and β for numerical reasons, and $[ClO_2^-]_0$ will be set equal to the intermediate value in the experimental range of concentrations of $NaClO_2$. Thus, the diffusion coefficient of the hydrogen ions is renormalized by the presence of the immobile carboxylic groups. The intrinsic value of the diffusion coefficients of hydrogen ions is an order of magnitude higher than that of the reactants, but its effective value can be dramatically reduced in a controlled way by adding an adequate quantity of sodium methacrylate polymer to the solution.

3. Materials and Methods

Throughout the experiments, reagent grade chemicals were used. The medium where the reaction−diffusion process took place was a thin layer of a viscous aqueous solution of polymer trapped between two flat glass plates separated by a 1.0 mm thick spacer. Among other things, the use of a viscous polymer avoids the development of undesired convective perturbations. The preparation bears some similarity to the one followed in ref 13, but we eliminated the cross-linking agent to avoid gelification. This allowed us to more easily cope with difficulties arising at the moment of incorporation of the reagents into the viscous medium. If the medium is solid the reagents, must be added by diffusion, a procedure that takes quite a long time. Moreover, the presence of a thin liquid layer of a reactive solution, between the plate and the surface of the gelified medium, could often be observed. This caused undesirable differences in the front propagation velocity at this interface. By working with a viscous solution susceptible to being stirred after polymerization, especially at the moment when the reactants were added, we ensured the homogeneity of the final preparation, and no additional interface is introduced between the medium and the covering plates. Two different polymer solutions were initially prepared: solution A, composed of a homopolymeric solution of acrylamide, and solution B, composed of heteropolymeric solutions of acrylamide and sodium methacrylate with the respective monomers in a ratio of 14 to 1. The initial composition of the mixture for the two different solutions is given in Table 1. These mixtures were left to polymerize at 0 °C for 2 h. The resulting highly viscous solutions were then washed from most remaining small solvated species by immersing a layer of these polymer solutions in a large

TABLE 1: Composition of Polymeric Solutions A and B

	A	B
water	85 mL	85 mL
acrylamide	21.32 g	19.9 g
sodium methacrylate	−	2.16 g
triethanolamine	0.75 g	
ammonium peroxidisulfate	0.24 g	
bromophenol blue	7.0×10^{-3} g	

volume of distilled water. After 12 h, the light fluid liquor at the top was gently poured out and the dense polymer rich solution at the bottom of the dish was kept for use. To establish the actual weight of the polymer content of the solution, a known amount of this latter viscous solution was removed and dried at 60 °C. The final amount of polymer in water was set equal in both of the viscous solutions by dilution. Solution B enabled us to incorporate controlled amounts of carboxylic groups (the binding agent for protons) into the reaction medium by mixing a weighed quantity of each of the viscous solutions.

Later, reactants and the pH indicator were added. We used sodium chlorite (Prolabo, 96% pure) and sodium tetrathionate (Sigma, 99% pure) as reactants. Bromophenol blue (10^{-5} M) was used as an indicator as it proved to be a very effective one, allowing us to visualize the front in a very clear way. Once the reactants and the indicator were added to the viscous medium, the solution was trapped between two glass plates and its borders were sealed to prevent evaporation, the end result being a 70 mm × 90 mm flat rectangular layer. A reaction−diffusion front was initiated in the middle of the rectangular layer by temporarily allowing the reactive solution to come into contact with a filter paper impregnated with an acid solution through a small hole (0.5 mm i.d.) bored through the uppermost glass plate; this hole was then subsequently sealed.

The concentration of carboxylic groups in the solution varied between 0 and 4.0×10^{-2} M, and the concentration of reactants varied between 5.0×10^{-4} and 1.0×10^{-2} M for the tetrathionate and between 2.0×10^{-3} and 4.0×10^{-2} M for the chlorite. The initial excess of chlorite to tetrathionate with respect the stoichiometric relation (I), ξ, was kept fixed and equal to 0.129 throughout all the experiments.

4. Experimental Results

Once the front was initiated by a small perturbation, it propagated at a decreasing velocity until reaching a stationary value. At this point, the effect of the destabilization on the front geometry began to be apparent. The front started at the center of the layer initially developed with circular geometry. Later this symmetry may be lost. We analyzed the behavior of the front in two different cases: (a) for constant values of reactant concentration and different concentrations of binding agent and (b) for constant values of carboxyl group concentration and varying reactant concentrations. First, we fixed the reactant concentration to evaluate the role of the binding agent in the development of instabilities. We observed that the mean propagation velocity decreased as the concentration of binding agent increased. Also, we could observe that for a solution prepared with a low concentration of carboxyl groups ($0-1.25 \times 10^{-2}$ M) the front preserved its circular symmetry and moved at a relatively high velocity. It was for a concentration of carboxyl groups higher than 1.25×10^{-2} M that the destabilization of the front began to be apparent. Keeping the reactant concentration fixed and varying that of the carboxyl groups, we could observe the continuation of the slowing effect and

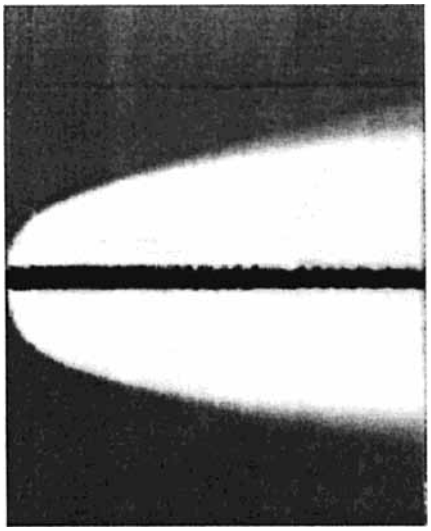

Figure 1. Time−space plot of a stopping front. The view size is 195 mm × 90 mm. Initial concentrations: $[NaClO_2]_i = 4.26 \times 10^{-3}$ M, $[Na_2S_4O_6]_i = 1.06 \times 10^{-3}$ M, and $[-COO^-]_i = 3.0 \times 10^{-2}$ M.

the beginning of the deformation of the fronts. For the lowest values ($1.25-1.5 \times 10^{-2}$ M), the circular fronts were only slightly deformed, losing their circular geometry but preserving their positive curvature. For concentrations between 1.5×10^{-2} and 2.0×10^{-2} M, the first neat cellular structures appeared.

If the concentration of carboxylic groups increased at the same time that the reactant concentration was kept fixed and low (5.0×10^{-4} to 5.0×10^{-3} M and 2.0×10^{-3} to 2.0×10^{-2} M for the tetrathionate and the chlorite, respectively), a circular front would begin to propagate, gradually slow, and eventually come to a stop at some critical radius. This is exemplified in the space−time plot in Figure 1. At this time, we recall that the system was closed. The stopping of the front was not due to a loss of capacity of the system to propagate R−D fronts with time, since a new circular front could be restarted at another location even when the first one was stopped.

The most interesting features appeared when we used a solution with higher values for both reactants and carboxylic groups. However, at some high reactant concentration, the reaction switched spontaneously to an acidic state during the preparation time, setting a practically higher limit to the reactant concentration that could be explored. Thus, we studied the evolution of the front when the concentration of carboxylic groups in the solution was 3.0×10^{-2} M and the reactant concentration varied between 5.0×10^{-2} and 1.0×10^{-2} M for the tetrathionate and between 2.0×10^{-2} and 4.0×10^{-2} M for the chlorite. We found that as the reactant concentration increased, the front mean velocity increased (as observed in ref 14) at the same time that the mean wavelength of the cellular structures decreased but the depth of the fiords between cells increased. We include in Figures 2 and 3 some images corresponding to different time steps of the evolution of a cellular front for a fixed concentration of carboxylic groups and different concentrations of reagents.

Another interesting feature observed during these experiences was the interaction between cellular fronts. Often, as time passed, some small imperfections at the border spontaneously trigger new R−D fronts that travel to an encounter with the front initiated at the center. This fact allowed us to study the interaction between colliding fronts. We observed that when the cellular structure developed, and only in that case, two colliding fronts would stop their advance at a certain distance separating them. That distance depended on the initial concen-

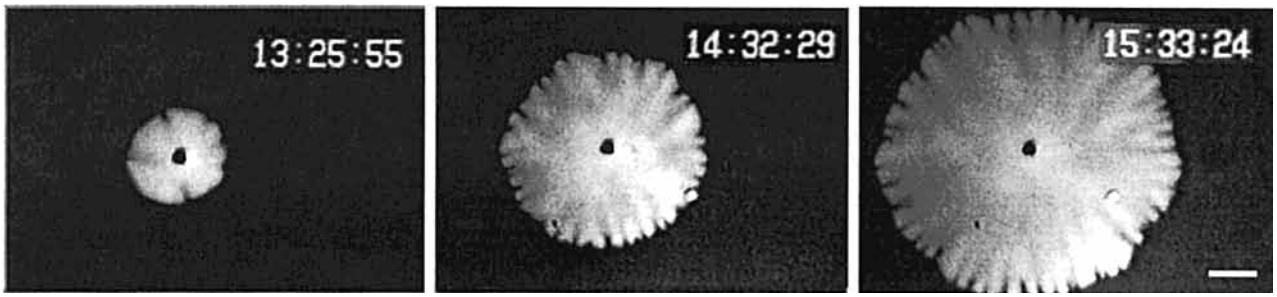

Figure 2. Evolution of a cellular front. Initial concentrations: $[NaClO_2]_i = 2.13 \times 10^{-2}$ M, $[Na_2S_4O_6]_i = 5.3 \times 10^{-3}$ M, and $[-COO^-]_i = 3.0 \times 10^{-2}$ M. The scale bar is 10 mm.

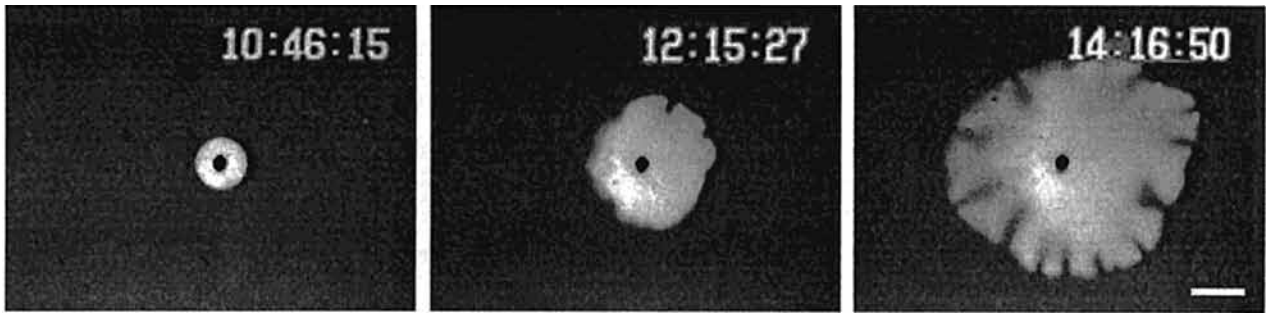

Figure 3. Same as Figure 2 with the following initial concentrations: $[NaClO_2]_i = 1.8 \times 10^{-2}$ M and $[Na_2S_4O_6]_i = 4.5 \times 10^{-3}$ M.

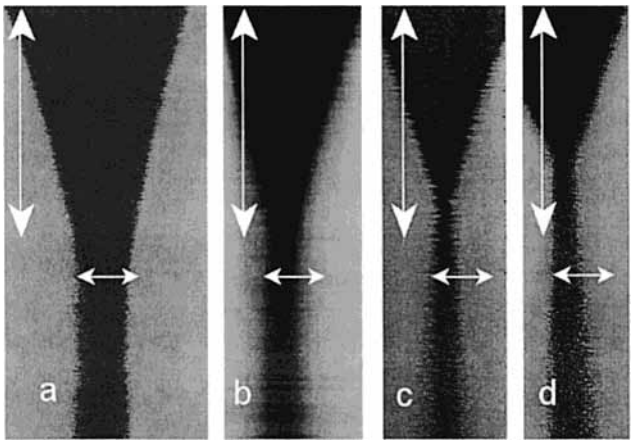

Figure 4. Time−space plot of a propagating front for several initial concentrations (and the scaled values for horizontal and vertical arrows): (a) $[NaClO_2]_i = 1.67 \times 10^{-2}$ M, $[Na_2S_4O_6]_i = 4.17 \times 10^{-3}$ M (1 cm, 700 min), (b) $[NaClO_2]_i = 1.8 \times 10^{-2}$ M, $[Na_2S_4O_6]_i = 4.5 \times 10^{-3}$ M (1 cm, 570 min), (c) $[NaClO_2]_i = 1.94 \times 10^{-2}$ M, $[Na_2S_4O_6]_i = 4.83 \times 10^{-3}$ M (1 cm, 450 min), and (d) $[NaClO_2]_i = 2.13 \times 10^{-2}$ M, $[Na_2S_4O_6]_i = 5.3 \times 10^{-3}$ M (0.25 cm, 230 min).

tration of reactants, being shorter for higher concentrations. At the same time, the behavior of the interacting fronts showed always the same features: a strong decrease in velocity and a slow smoothing of the cellular structures. In Figure 4, we show a time−space plot of a very thin slice of the bidimensional pattern for several cases, where the change in velocity can be observed. The fronts traveled with constant velocity until they came to a certain distance where they began to interact and stopped. After a certain time, the distance separating those fronts apparently began to grow again as if they bounced back. This may seem paradoxical since, here, we are dealing with a closed system where major reagents are consumed in one shot. Actually, this fact may be simply accounted for by the diffusive process, when the reaction process comes to a quasi-stop. In the next section, we will discuss the numerical analogies corresponding to each one of the aspects presented in this section.

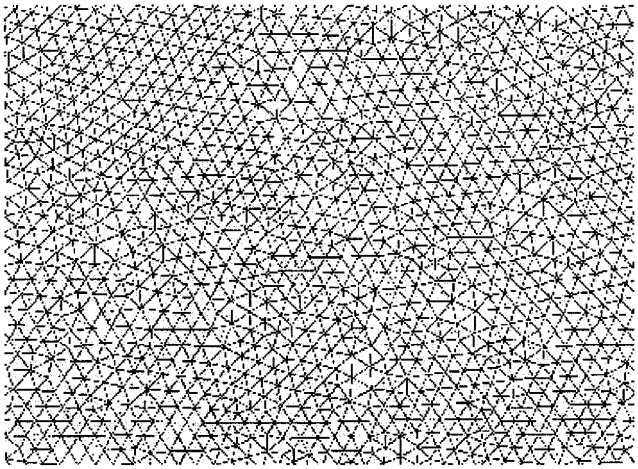

Figure 5. Section of the triangular mesh used for the numerical simulations.

5. Numerical Results

We have performed our numerical simulations using a standard finite element scheme. We used triangular elements with a length h of $\simeq$0.1 and a time increment Δt of 0.05. Neither perturbations nor fluctuations were added but that corresponding to numerical noise due to the implicit irregularity of the triangular mesh (see Figure 5).

The values for the parameters where chosen for comparison of experimental and numerical results. First, we analyzed the effects of K on the stability of a circular front. We found that for small K values (low concentrations of methacrylate), the front developed and moved, preserving its circular geometry and smooth boundaries. As K increased, the instabilities appeared, turning the front irregular and slower. Then, K was set equal to 100, according to eq 3, with a typical experimental value for $[-COO^-]$ of 1.0×10^{-2} M which would correspond to a pK_a value of 4, a typical value for organic acids such as methacrylic acid. We adopted a $[ClO_2^-]_0$ of 1.5×10^{-2} M for α and β in eq 7. We analyzed the effects of reactant concentration (α in eq 7) on the stability of a circular front. The numerical

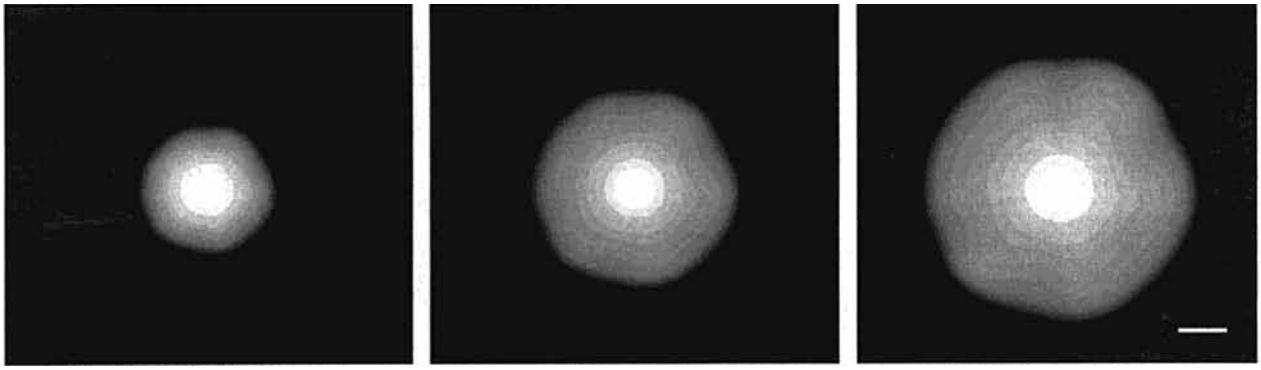

Figure 6. Numerical simulation for the development of a cellular front. Initial conditions: $[NaClO_2]_i/[NaClO_2]_0 = 0.75$. $[NaClO_2]_0 = 1.5 \times 10^{-2}$ M. Normalized time interval of 180 min. The scale bar is 10 mm. $K = 100$.

Figure 7. Same as Figure 6 with $[NaClO_2]_i/[NaClO_2]_0 = 1.25$. Normalized time interval of 60 min.

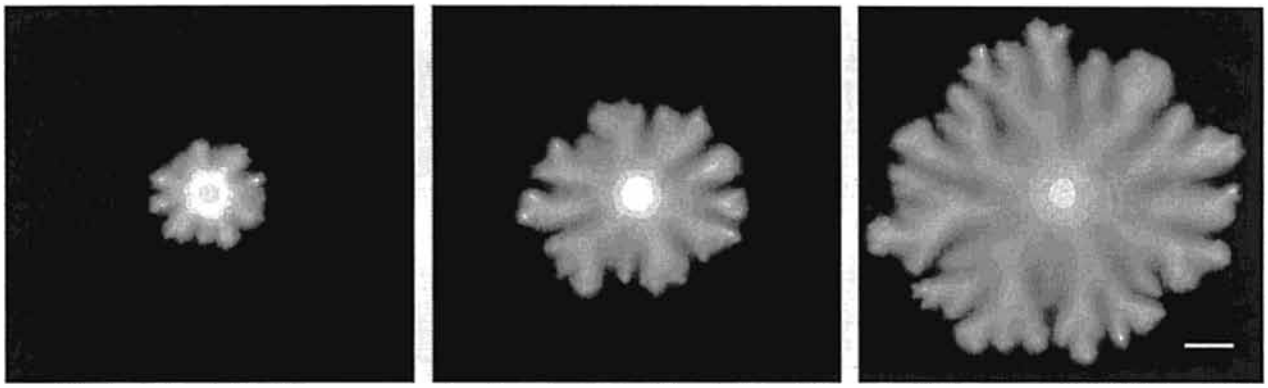

Figure 8. Same as Figure 6 with $[NaClO_2]_i/[NaClO_2]_0 = 1.5$. Normalized time interval of 35 min.

results, analogous to the experimental observations depicted in Figures 2 and 3, are shown in Figures 6−8. As during the experimental situation, the higher the concentration of reactants was, the longer and thinner the peninsulas developed by the instabilities became. For higher values of K and correspondingly of α, similar results were obtained.

Second, we searched for a "stopping front" effect for a determined concentration of reactants and binding agents. Experimentally, we observed that under certain conditions a circular front moves until reaching a defined radius. We looked for the same situation numerically and found that when the front was circular, after traveling for some distance, it could stop itself and preserve its size over a long time (compared with evolution time).

Last, we analyzed the behavior and interaction of two planar fronts traveling toward an encounter line. We found that the interaction between fronts made them stop at a distance that became shorter as the concentration of reactants increased. As found experimentally, when the interaction between the cellular fronts began, the velocity of propagation rapidly decreased to almost zero and the lateral instabilities were smoothed out, almost allowing a regular planar boundary between both fronts. In Figures 9 and 10, we show a pair of propagating fronts and the normalized position in time of the interfaces between the basic and acidic state denoted by $x_i([H^+]_c)$, where $i = 1$ or 2 for the right-hand or left-hand front, respectively.

When the scaled values for the initial concentration of reactives are considered, the calculated propagation velocities fit very well the experimentally observed values. The same is true for the final calculated H^+ concentration.

6. Conclusion

We presen the different experimental aspects of the propagation and interaction of cellular acidity fronts in a closed system and compared them with numerical results obtained by simulations of an overall rate equation for the reaction. For each experimentally observed features, we could reproduce a corresponding numerical analogue feature.

From the point of view of experimental results, we want to emphasize the following aspects. The utilization of a very viscous solution instead of a solid gel produces more dramatic

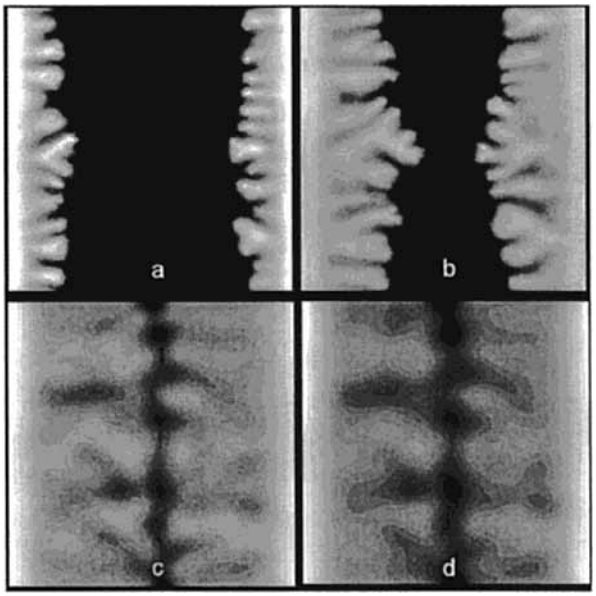

Figure 9. Numerical simulation of the propagation and interaction of two initially planar fronts. Initial conditions: $[NaClO_2]_i/[NaClO_2]_0 = 1.5$. $[NaClO_2]_0 = 1.5 \times 10^{-2}$ M. Normalized time interval of 40 min. Normalized view size of 8 cm × 8 cm.

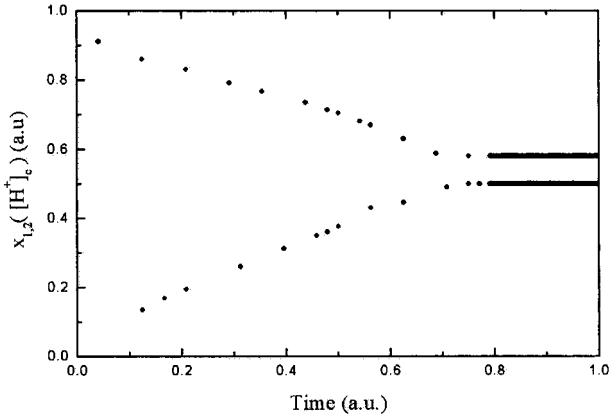

Figure 10. Time−space plot of the propagating fronts of Figure 9. $x_1([H^+]_c)$ and $x_2([H^+]_c)$ are the right- and left-hand fronts, respectively.

results from the point of view of the development of cellular fronts. The existence of these fronts depends strongly on the effective diffusion ratio between the reactants and the catalyzer, as predicted theoretically and observed experimentally in this and previous works.[11] The destabilization of a flat front is gradually amplified by the addition of a polyelectrolyte, reducing the extent of diffusion of the hydrogen ion. This feature was observed experimentally and numerically.

The shape behavior of the cellular front, as the diffusivity of the catalyst is reduced, was the same both in the experiments and in the simulation. Initially, the manifestation of the instability is almost imperceptible, the front being slightly deformed. As the concentration of binding agent is increased, the cellular front develops more apparently. Fixing the concentration of binding agents, we studied the effect of the initial concentration of reactants, finding that as this concentration was increased a finer structure with sharper and narrower fiords appeared. This fact is in close agreement with what was observed for the interaction between two cellular fronts. The distance at which a traveling front stops because of the interaction with another one traveling in the opposite direction decreased as the initial concentration of reactants was increased. As a consequence, the distance between the perturbations of the fronts that will survive and be amplified is smaller for higher concentrations of reactants, leading to the formation of smaller and sharper cellular structures on the front. When neither the development of the cellular front nor the interactive stopping behavior between fronts was possible, every encounter between two of them resulted in a collision. The apparent pull-back of two fronts after their halt at a distance is simply due to the diffusive erosion of the standing front structure. This is clearly observed and understood in numerical simulations.

Another interesting feature is the fact that within a certain range of concentrations of reactants and binding agents an initially moving circular front will stop after reaching a critical radius. This behavior should be analyzed taking into account the effect of the curvature of the front on the stationary profile of the interface in a closed system.

To summarize, we want to emphasize the close correspondence between numerical and experimental results despite the relative crudeness of the kinetic description of the reaction. The calculated distances and velocities were of the same order of magnitude. Similar cellular front instabilities have also been observed using thiosulfate instead of tetrathionate. However, the kinetic mechanism of the reaction between thiosulfate and chlorite is much more complex[15] and thus more difficult to associate with a tractable model. Studies of the reaction system in an open spatial reactor have been performed and will be the subject of a further publication.

Acknowledgment. We thank G. Buscaglia and E. Dari for providing the algorithm package used in the numerical analysis and J. Boissonade for stimulatig discussions. M.N.K. and M.F. thank Fundación Antorchas for partial support.

References and Notes

(1) Kapral, R., Showalter, K., Eds. *Chemical Waves and Patterns*; Kluwer Academic Publishers: Dordrecht, The Netherlands, 1994.

(2) Jensen, O.; Pannbaker, V. O.; Dewel, G.; Borckmans, P. *Phys. Lett.* **1993**, *A179*, 91. Jensen, O.; Pannbaker, V. O.; Mosekilde, E.; Dewel, G.; Borckmans, P. *Phys. Rev. E* **1994**, *50*, 736. Métens, S. Ph.D. Thesis, Université Libre de Bruxelles, Brussels, Belgium, 1998.

(3) Hagberg, A.; Meron, E. *Phys. Rev. E* **1993**, *48*, 705. Hagberg, A.; Meron, E. *Nonlinearity* **1994**, *7*, 805. Hagberg, A.; Meron, E.; Rubinstein, I.; Zaltman, B. *Phys. Rev. E* **1997**, *55*, 4450.

(4) Pearson, J. E. *Science* **1993**, *261*, 189.

(5) Castets, V.; Dulos, E.; Boissonade, J.; De Kepper, P. *Phys. Rev. Lett.* **1990**, *64*, 2953. Perraud, J. J.; De Wit, A.; Dulos, E.; De Kepper, P.; Dewel, G.; Borckmans, P. *Phys. Rev. Lett.* **1993**, *71*, 1272. De Kepper, P.; Perraud, J. J.; Dulos, E. *Int. J. Bifurcation Chaos Appl. Sci. Eng.* **1994**, *4*, 1215. Dulos, E.; Davies, P. W.; Rudovics, B.; De Kepper, P. *Physica D* **1996**, *98*, 53.

(6) Ouyang, Q.; Swinney, H. L. *Nature* **1991**, *352*, 610. Ouyang, Q.; Noszticzius, Z.; Swinney, H. L. *J. Phys. Chem.* **1992**, *96*, 6773.

(7) Lee, K. J.; McCormick, W. D.; Ouyang, Q.; Swinney, H. L. *Science* **1993**, *261*, 194. Lee, K. J.; Swinney, H. L. *Phys. Rev. E* **1995**, *57*, 1899. Lee, K. J.; Swinney, H. L. *Int. J. Bifurcation Chaos Appl. Sci. Eng.* **1997**, *7*, 1149.

(8) Ortholeva, P.; Ross, J. *J. Chem. Phys.* **1974**, *60*, 5090.

(9) Kuramoto, Y. *Chemical Oscillations, Waves and Turbulence*; Springer-Verlag: Berlin, 1984.

(10) Horváth, D.; Petrov, V.; Scott, S. K.; Showalter, K. *J. Chem. Phys.* **1993**, *98*, 6322.

(11) Horváth, D.; Showalter, K. *J. Chem. Phys.* **1995**, *102*, 2471.

(12) Davies, P. W.; Blanchedeau, P.; Dulos, E.; De Kepper, P. *J. Chem. Phys.* **1998**, *102*, 8236.

(13) Toth, Á.; Lagzi, I.; Horváth, D. *J. Phys. Chem.* **1996**, *100*, 14837.

(14) Toth, Á.; Horváth, D.; Siska, A. *J. Chem. Soc., Faraday Trans.* **1997**, *93*, 73.

(15) Nagypal, I.; Epstein, I. R. *J. Phys. Chem.* **1986**, *90*, 6285.

(16) Szirovica, L.; Nagypál, I.; Boga, E. *J. Am. Chem. Soc.* **1989**, *111*, 2842.

(17) Epstein, I. R.; Lengyel, I. *Proc. Natl. Acad. Sci. U.S.A.* **1992**, *89*, 3977.

(18) Horváth, D.; Toth, Á. *J. Chem. Phys.* **1998**, *108*, 1447.